Molecular Catalysis 533 (2022) 112797

Contents lists available at ScienceDirect

Molecular Catalysis

journal homepage: www.journals.elsevier.com/molecular-catalysis

Carbon supports for the oxidative cleavage of oleic acid: Influence of textural properties

Sebastián Gámez [a,*], Ernesto de la Torre [b], Eric M. Gaigneaux [a]

[a] Institute of Condensed Matter and Nanosciences, Université Catholique de Louvain, Place Pasteur 1, L4.01.09, Louvain-la-Neuve 1348, Belgium
[b] Department of Extractive Metallurgy, Escuela Politécnica Nacional, Ladron de Guevera E11-253, Quito 170517, Ecuador

ARTICLE INFO

Keywords:
Activated carbon
Carbon black
Fatty acids
Heterogeneous catalysis
Oxidative cleavage

ABSTRACT

Microporous oxidized activated carbon (ACO) and macroporous oxidized carbon black (CBO) were assessed in the complexation of Ru for the oxidative cleavage of oleic acid. This reaction breaks carbon-carbon double bond to produce azelaic and pelargonic acids (highly demanded in pharmacology). Both carbon materials were treated with HNO_3 prior Ru deposition by wet impregnation method. Carbon supports were characterized by FTIR, Boehm's titration and N_2 physisorption, while Ru complexation was determined by ICP and XPS spectroscopy. Activated carbon catalyst displayed a low conversion (~53%) in comparison to carbon black catalyst (>99%). The reason is related to the molecular length of oleic acid (2.2 nm), estimated by *ab initio* Hartree-Fock calculation, which is larger than micropores from activated carbon (~0.7 nm). Despite Ru losses during the catalytic tests, CBO was more active and stable than ACO, confirming that a macroporous support is more suitable to perform the oxidative cleavage of oleic acid.

1. Introduction

Since many years, carbon materials have been exploited as supports for the preparation of heterogeneous catalysts due to their flexibility at the moment to tailor their physical and chemical properties [1]. For instance, through chemical activation at various temperatures with different activating agents such as H_3PO_4 and alkali metal compounds (e.g. KOH or NaOH), it is possible to develop a large surface area, being the first step to facilitate the dispersion of active species [2]. Moreover, pore size distribution can be tuned in order to improve the diffusion of reactants and products to and from the surface. Chemical treatments involving strong acids (e.g. HNO_3 or H_2SO_4) or oxidizing agents (e.g. $KMnO_4$) are commonly used to increase the number of chemical functionalities suitable to chelate transition metal cations [3,4]. In the literature many examples are reported of different carbon materials as catalyst supports. Mainly activated carbon (AC), carbon black (CB), carbon nanotubes (CNTs) and graphene have been widely exploited in the field of heterogeneous catalysis [5]. For instance, CNTs have been used in several applications from photocatalysis to recent open research areas like electrocatalysis (e.g. water splitting) [6].

Besides the mentioned properties, carbon materials present additional important advantages over other traditional supports. Amid them, their resistance to acidic and alkaline media makes carbons suitable for several catalytic applications in all pH range [1,7]. One of these catalytic applications where carbon materials can be used, is the oxidative cleavage reaction. The latter involves the rupture of carbon-carbon double bonds of different alkenes using a transition metal in a high oxidation state (e.g. Ru, Os, W) [8] along with a strong oxidizing agent (e.g. $NaIO_4$) [9]. In the specific case of unsaturated fatty acids (UFAs), the oxidative cleavage reaction is applied to oleic acid (the most abundant UFA in nature) to produce pelargonic (PA) and azelaic (AA) acids which are valuable products for herbicides and cosmetics preparation, respectively [10]. In literature, most of the works employ Ru homogeneous catalysts because of their high activity and selectivity in this reaction [8]. Briefly, a Ru precursor salt is transformed into $Ru(VIII)O_4$ species with the aid of $NaIO_4$ to cleave the carbon-carbon double bonds via a pericyclic [3+2] reaction [11]. The two carbonyl intermediates formed are over oxidized by means of $NaIO_4$ to yield the final carboxylic acids [11]. However, very few examples of heterogeneous catalysts have been published because of the poor conversions and yields obtained in this reaction [8].

In this regard, oxidation reactions have been largely scoped by carbonaceous materials as is the case of activated carbon [12,13]. This microporous carbon support possesses a high specific surface area as

* Corresponding author.
E-mail address: sebastian.gamez@uclouvain.be (S. Gámez).

https://doi.org/10.1016/j.mcat.2022.112797

Available online 12 November 2022

consequence of an activation process [2]. Commonly biomass lignin derivatives are carbonized at 600 °C under reducing atmosphere followed by a further activation process consisting in a heating at 900 °C under CO_2 or H_2O atmosphere. Under these conditions, CO_2 and/or H_2O vapor diffuse into the carbon matrix to react with carbon atoms generating CO/H_2 as well as porosity [14,15]. The shape and size of the pores in AC mainly depend on the morphological, chemical and physical properties of the raw materials used as well as the kind of activation process employed [14,15]. Afterwards, a well-developed surface area with numerous oxygenated functional groups such as carboxylic acids, phenols, carbonyls and lactones can facilitate the adsorption of several transition metal ions widely used in catalysis [14]. Additionally, its high surface area, due to a well-developed porosity, contributes to high metal dispersions which is essential for high catalytic activity [16].

Another carbonaceous material used as a support in oxidation reactions is carbon black (CB) [17,18]. This carbon material has been mainly employed in the tire industry as a reinforcement in rubbers or as ink pigment and additive for coatings and polymers [17]. For instance, it is added to elastomers to enhance their mechanical performance [19]. Generally, carbon black is produced from the incomplete combustion of heavy petroleum products such as coal tar or liquid hydrocarbons [20]. This type of material tends to form aggregates (nodules) as a consequence of an agglomeration of carbon black particles [20]. According to the aggregation degree of carbon black nodules it is possible to obtain high or low dispersive materials. Besides, this aggregation capacity of carbon black spherical particles influences directly their surface area. Precisely, small particles normally promote high surface areas whereas a high degree of particles aggregation yields low surface areas [19].

As catalyst support, CB is preferable than other carbon materials such as carbon nanofibers or graphene for its accessibility and low cost. One of the main characteristics that makes CB attractive for catalytic applications, is its high surface area/volume ratio which is due to the small size of the spherical particles (approximately 50 nm) [21]. Other important characteristic of this carbon material is the presence of oxygenated groups which could be originated from the fabrication process or be incorporated in a subsequent oxidation treatment [22,23]. The modification of the CB surface chemistry may enhance the impregnation of several transition metals which can be used as catalyst for different applications such as alcohols oxidation, hydrogen generation or hydrolytic hydrogenation of cellulose [24–26].

In spite of all aforementioned positive characteristics and properties of carbon materials, examples of oxidative cleavage of alkenes using these supports is extremely rare. Kumar et al. impregnated Ru on charcoal (Ru load= 5 wt%) to perform the oxidative cleavage of various alkenes and alkynes using oxone as oxidizing agent [27]. High conversions were obtained in short reaction times when small alkenes (aliphatic or aromatic) were assessed. Nevertheless, so far no UFAs have been analyzed with catalytic carbon systems. Therefore, in this article apart to synthesize Ru-carbon heterogeneous catalysts and measure their stability against leaching issues, the influence of two carbon materials with different textural properties (AC and CB) was studied in the oxidative cleavage of oleic acid (C8:1). The main purpose was to verify the influence of different surface areas and pore sizes on the scission of a carbon-carbon double bond of a large UFA and how a functionalization process (i.e. oxidation with HNO_3) may enhance the capability of carbon supports to retain Ru on their surface assuring better stability for further catalytic tests. Through this assessment, it will be possible to identify a suitable carbon material for this reaction.

2. Experimental

2.1. Materials

Activated carbon (AC, coconut shell, 2–4 mm, basic, specific surface area~ 1000 m^2/g and pore volume 0.45 cm^3/g) was purchased from Calgon Corporation while carbon black (CB) was purchased from Degussa Printex ®G (95.73 wt% C, 0.73 wt% H, 3.5 wt% O, mean particle size = 27 nm, specific surface area 154 m^2/g and pore volume 0.56 cm^3/g). Heptanoic acid (Internal standard, $C_7H_{14}O_2$, >98% GC), pelargonic acid (PA, $C_9H_{18}O_2$, >98% GC) and azelaic acid (AA, $C_9H_{16}O_4$, >98% GC) were obtained from TCI chemicals. Ruthenium(III) chloride hydrate, 99.9% (PGM basis) ($RuCl_3.H_2O$, Ru 38%) was purchased from Alfa Aesar. Sodium metaperiodate ($NaIO_4$, >99%) was obtained from Sigma-Aldrich. Acetonitrile (MeCN, C_2H_3N >99.98% GC), oleic acid (OA, $C_{18}H_{34}O_2$, >99.9% GC), nitric acid (HNO_3 > 65%) and ethyl acetate (AcOEt, $C_4H_8O_2$ > 99.9% GC) were purchased from Carl Roth. Sodium nitrate ($NaNO_3$, >99%) was purchased from Merck while potassium bromide for spectroscopy (≥99%) was obtained from Acros Organics.

2.2. Preparation of carbon materials

Activated carbon (AC) and carbon black (CB) were submitted to an oxidation treatment with nitric acid in order to incorporate oxygenated functional groups (phenols, lactones and carboxylic acids) on their surfaces [28–31]. For this purpose, a 150 mL round flask was used to add 4 g of AC/CB in 50 mL of 5.0 M HNO_3 solution. The suspension was magnetically stirred (1500 rpm) and heated at 90 °C for 8 h under reflux in order to avoid nitric acid losses. As regards AC, agitation speed was maintained at 500 rpm to avoid an excessive attrition of the carbon matrix. Afterwards, oxidized activated carbon (ACO) was filtered to recover the solid on a Whatman filter paper while oxidized carbon black (CBO) was separated from the solution by centrifugation at 14,000 rpm (26,200 g) during 20 min in a Heraeus MultifugeX1R centrifuge. Both carbon materials were washed in a Soxhlet equipment for 48 h in order to remove all nitric acid remainings inside the carbonaceous matrix. Finally, oxidized carbon supports were dried for 48 h at 110 °C to ensure removal of the remaining water inside the carbonaceous materials.

2.3. Synthesis of Ru-carbon catalysts

Normally, 500 mg of CBO (mean particle size after oxidation = 23 nm) was added into 20 mL of distilled water and further dispersed by ultrasonic treatment for 15 min. In the case of ACO, the suspension was not submitted to ultrasounds since ACO grains size was in a 2–4 mm range. Afterwards, 10 mL of $RuCl_3$ solution (10 mM) was added drop by drop to the above suspension under magnetic stirring for the next 24 h in order to achieve a Ru load of 2 wt%. Finally, the solids were recovered by filtration and centrifugation in the case of ACO and CBO, respectively. Henceforth, oxidized activated carbon with Ru is denoted as ACO-Ru(2%) whereas oxidized carbon black catalyst is denoted as CBO-Ru(2%).

2.4. Characterization

Morphology of carbon supports was observed by means of scanning electron microscope (SEM) JEOL JSM-7600F with an accelerating voltage of 0.1–30 kV. Secondary electron images (SEI) were acquired with a resolution of 1.5 nm (1 kV). Optical microscopy was also employed using a microscope Olympus SZX16. For the estimation of AC particle size, a granulometric analysis (ASTM D2862) was performed through sieving the material with a series of sieves of different opening sizes [32]. Particle size was determined by d_{80} indicator (see Table S1) which refers to the mesh opening of the sieve through which 80% of the carbon material passed [33]. Particle size distribution of carbon black materials were determined by transmission electron microscopy (TEM) in a LEO 922 microscope with an acceleration voltage of 200 kV and equipped with a LaB6 thermal cathode. From each acquired image, the diameter of 20–25 particles was measured in order to obtain the mean particle size and the standard deviation after building a frequency distribution histogram.

Fourier transform Infrared spectroscopy (FTIR) was performed to

characterize the different carbon supports employed in this research work. For this purpose, wafers were prepared by mixing 15 mg of sample with 300 mg of KBr beforehand dried overnight at 110 °C. All analyzes were carried out in a Bruker Equinox 55 FTIR spectrometer in the transmission mode. One hundred scans were carried out in the range of 4000–400 cm^{-1} with a 4 cm^{-1} resolution. Boehm's titration was also conducted to quantify the amount of oxygenated groups AC and CB. For this purpose, three samples of 0.5 g were added to three 0.05 M solutions of NaOH, Na_2CO_3 and $NaHCO_3$ (50 mL each one). The suspensions were degassed for 1 h under argon atmosphere and stirred for other 23 h. Then, the solids were separated by vacuum filtration with the aid of a filter paper (pore size: 0.2 μm). Next, 10 mL of the filtrate was taken from each suspension and were acidified with 20 mL of a 0.05 M HCl solution. The new solutions were agitated and continuously degassed for 2 h under argon atmosphere. Finally, the solutions were titrated using a 0.05 M NaOH solution with phenolphthalein as indicator [34,35]. The three basic solutions allow to measure different oxygenated groups on carbon surfaces. Precisely, NaOH neutralizes all acidic functional groups of the in phenols, lactones and carboxylic types. Na_2CO_3 neutralizes lactones and carboxylic groups, whereas $NaHCO_3$ neutralizes only carboxylic groups. By subtracting the results obtained with each base, the amount of phenols, lactones and carboxylic groups on carbon materials can be estimated [34,35].

Additionally, the point of zero charge (PZC) was estimated. This indicator corresponds to the pH where there is not charge (whatever negative or positive) at all at the surface of the material [36,37]. Thus, at a pH below PZC the surface will be positively charged while over this value the surface will be negatively charged. PZC of both carbon materials was estimated by means of the Mass Titration method. Precisely, the pH of a 50 mL (0.1M $NaNO_3$) solution was registered using a Hanna Checker® portable pH meter. Then, 0.2 g of each sample was immersed within the solution and stirred up to 2 h or until pH of the solution did not change. The pH of the suspension was registered and then other 0.2 g of the same material was added again. This process was repeated until the pH of the suspension did not change anymore and the final value corresponds to the PZC [38].

The textural properties of all carbon materials were determined by N_2 physisorption at -196 °C in a Micromeritics Tristar 3000 equipment. Before the analysis, 50 mg of sample was degassed overnight under vacuum (~10.7 Pa) at 150 °C. The total surface area was calculated by the Brunauer-Emmet-Teller (BET) method using the adsorption isotherm in the partial pressure (P/Po) range from 0.05 to 0.30. In the case of activated carbon (microporous material), a lower P/Po range from 0.004 to 0.08 was employed for the BET method application [39]. In addition, the t-plot method was used to estimate the external surface area by the slope of the line drawn in the linear portion of $0.3 < P/Po < 0.8$. The micropore volume was determined after multiplying the intercept of the t-plot (in mol/g) by the density conversion factor = 0.001547 (when cm3/mol in the Y axis) or 34.53496 cm^3/mol (when mol/g in the Y axis) [40]. The micropore specific surface area was estimated by the difference between the BET area and the external surface area while the total pore volume was measured at P/Po = 0.98. Pore size distribution was estimated by Barrett, Joyner and Halenda method (BJH) using the data from the desorption isotherm branch [39,41]. For microporous materials the micropore volume was estimated with the Dubinin-Radushkevich (DB) method in a $P/Po < 0.1$ range whereas micropore size distribution was estimated by means of the Horvath-Kawazoe (HK) method [42,43].

X-ray photoelectron spectroscopy (XPS) was employed to verify Ru chemical environment on synthesized catalysts and to estimate the oxidation state of Ru. The analyzes were carried out in a SSX 100/206 photoelectron spectrometer from Surface Science Instruments (USA) equipped with a monochromatized micro focused Al X-ray source (powered at 20 mA and 10 kV). The pressure in the analysis chamber was around 10^{-9} Pa and the flood gun was set at 8 eV. The angle between the surface and the axis of the analyzer lens was 55° The analyzed area was approximately 1.4 mm^2 and the pass energy was set at 150 eV. Under these conditions, the full width measured at half maximum (FWHM) of the Au $4f_{7/2}$ peak for a clean gold standard sample was about 1.6 eV. Samples were prepared by pressing the powder in small stainless steel troughs of 4 mm diameter and placed on a ceramic carousel with a Ni grid which was set above the sample surface for charge stabilization. The following sequence of spectra was recorded: survey spectrum, C 1s, O 1s, N 1s, Cl 2p, Ru 3p. For all samples, C 1s spectrum was recorded again to check the stability of charge compensation with time. The aromatic C-(C,H) component of the C1s peak of carbon was fixed at 284.8 eV to set the binding energy scale. Data treatment was performed with the CasaXPS program (Casa Software Ltd, UK). The identification and quantification of Ru was performed with the $3p_{3/2}$ peak in order to avoid deconvolution problems associated with the C 1s peak (C 1s and Ru $3d_{5/2}$ peaks have similar binding energies) [44].

Ru load on each catalyst was determined through ICP-AES spectrophotometry in a ICP 6500 Thermo Scientific Instrument. About 100 mg of each sample were mixed along with 1 g of NaOH and Na_2O_2 and melted on the flame of a Bunsen burner. Then, samples were acidified with HCl and diluted with distilled water in order to be analyzed. Ruthenium dispersion was measured by CO chemisorption in a Micromeritics PulseChemiSorb 2705. It is important to mention that the information obtained by this technique is only indicative of the distribution of Ru on the carbon surface. Samples of 0.25 g were reduced at 200 °C under hydrogen atmosphere for 2 h (Air liquid; Purity > 99.999%) with a heat ramp of 10 °C/min. After reduction, helium (Air liquid; Purity > 99.999%) was passed through for 1 h until the temperature decreased to 35 °C. Under these conditions, CO pulses (20% of CO in Helium as carrier gas) were introduced. A TCD detector was employed to estimate the CO moles not adsorbed by Ru and thereafter to estimate Ru dispersion. Under the analysis conditions, metallic ruthenium on the surface adsorbs CO molecules with a stoichiometric ratio of Ru:CO=1:1 [45].

2.5. Catalytic tests

For this purpose, 0.5 mmol (141 mg) of oleic acid (OA) was dissolved in a biphasic solution of H_2O/MeCN/AcOEt (8/4/2 mL) along with 4 and 8 equivalents of $NaIO_4$ (Scheme 1). Heptanoic acid (81.7 μL) was also introduced in the reaction mixture as internal standard (IS). Then, 100 mg of each Ru-carbon catalyst was added to the reactor and the suspension was magnetically stirred at 1500 rpm for 24 h at room temperature (~18 °C). Samples from organic phase were extracted at different time intervals to monitor the reaction by gas chromatography in a Varian 3800 Gas Chromatograph equipped with a Flame Ionization Detector (FID) and a Stabilwax-DA Restek column, formed by a crossbond acid-deactivated Carbowax polyethylene glycol as stationary phase. After 24 h of stirring, three subsequent extractions from the aqueous phase were conducted with ethyl acetate to recover all the pelargonic (PA) and azelaic acid (AA) that could have formed an emulsion in the aqueous phase. The calculation of conversion, yields and selectivity are detailed in the Supporting information section.

Recycling tests were performed to verify the catalytic stability of the synthesized Ru-carbon catalysts. When a catalytic test was finished, the solid catalyst was separated from the biphasic solution by centrifugation in a Heraeus MultifugeX1R Centrifuge at 14,000 rpm (26,200 g) for 30 min. The solid catalyst was washed three times with warm distilled water (~80 °C) and dried overnight at room temperature. Next, the used catalyst was added in a fresh reaction mixture to start again the oxidative cleavage of oleic acid with the procedure explained before. This procedure was repeated five times to verify changes in catalytic activity after each recycle test.

Finally, hot-filtration tests were conducted to verify the possibility of Ru leaching. When conversion in a catalytic test reached ~50%, the solid catalyst was removed from the reaction medium by centrifugation in a Heraeus MultifugeX1R Centrifuge at 14,000 rpm (26,200 g) for 30

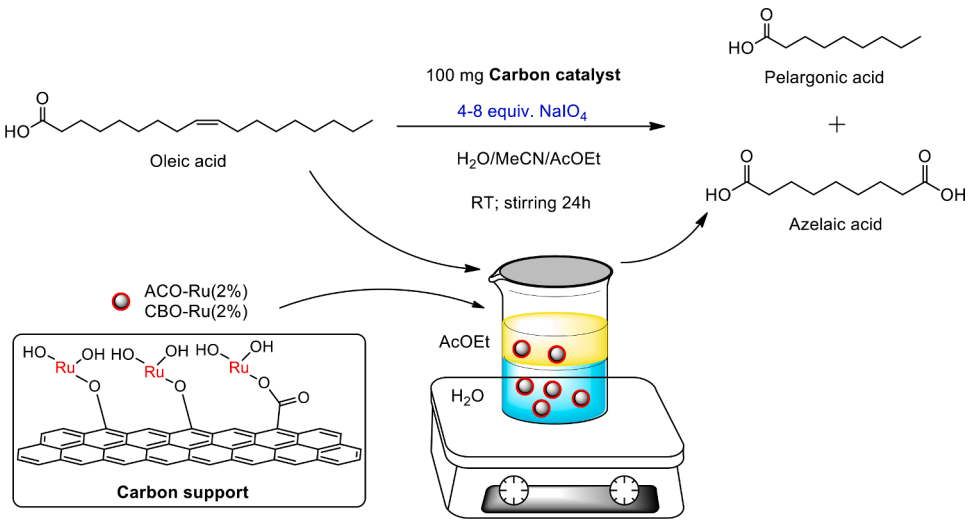

Scheme 1. Oxidative cleavage tests carried out with ACO-Ru(2%) and CBO-Ru(2%) catalysts.

min. Then, the reaction (liquid phase) continued to be monitored (without the solid catalyst) by injecting samples of the organic layer in the chromatograph. By this mean, it was possible to verify if there was catalytic activity after solid catalyst removal. An increase in conversion would suggest that Ru have dissolved in the liquid phase.

3. Results and discussion

3.1. Characterization

Fig. 1a and b show SEM images of activated carbon grains before and after the oxidation treatment, respectively. The ACO surface (Fig. 1b) shows some fractures which is an evidence that the treatment with HNO_3 caused damages to the carbonaceous matrix. On the other hand, the agglomeration of carbon black nodules was not disrupted after the oxidation with HNO_3. As regards mean particle size obtained from TEM images (Fig. S1c and d), particle size distribution of CB and CBO are barely modified (27 nm and 23 nm, respectively). It is worth to mention that the conditions specified in the Experimental section were already the optimized ones. When higher concentration of HNO_3 was employed or longer exposing times were tested, AC grains started to break and they were recovered in form of powder requiring longer washing periods in the Soxhlet equipment to get rid of HNO_3 remainings. Similarly, when $>$ 5 M HNO_3 was used, intense centrifugation (times $>$ 1 h) was necessary to recover the tiny carbon black nanoparticles produced because of nodules rupture. In fact, it was not possible to use these CBO nanoparticles in catalytic tests because it was impossible to separate them from the aliquot before injection in the GC. The mean particle size calculated for both carbon materials confirms that they maintained their initial particle size in spite of the oxidation treatment under the

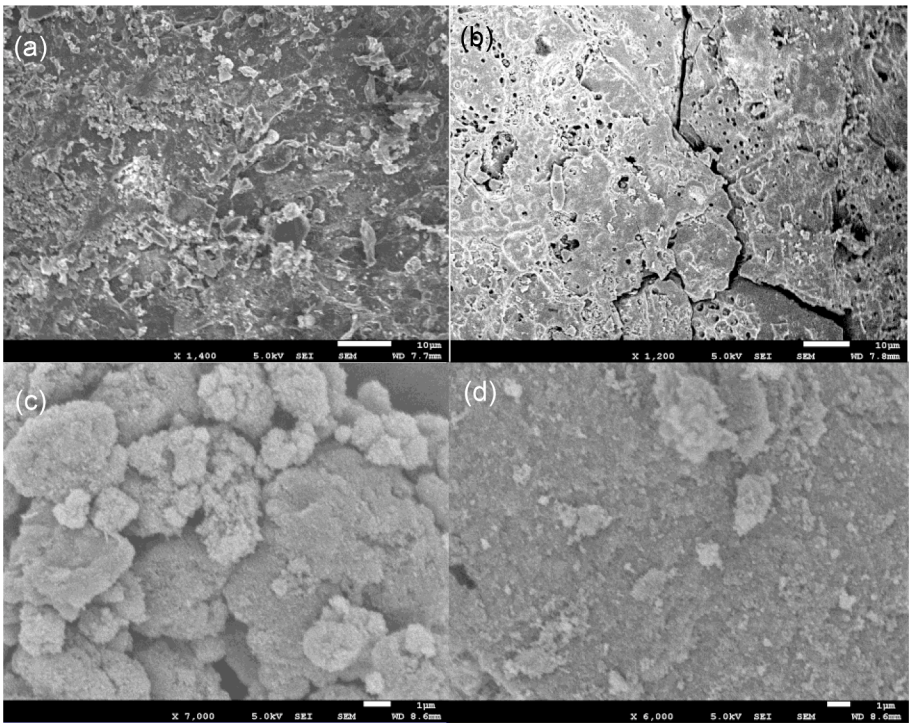

Fig. 1. SEM images of: (a) AC, (b) ACO, (c) CB and (d) CBO.

optimized conditions employed.

Fig. 2 shows the IR spectra of activated carbon and carbon black. As regards AC, an intense band appears at 3440 cm^{-1} which belongs to O—H stretching vibration mode in hydroxyl groups [46]. A thin peak was observed at 1640 cm^{-1} which is characteristic of carbon materials and attributed to C=C stretching vibration in aromatic rings [47,48]. A broad band at 1200 cm^{-1} is attributed to C—O stretching vibration in lactone groups while the wide band at 767 cm^{-1} can be ascribed to C—H out-of-plane bending in the aromatic rings [48,49]. In the case of ACO the same peaks were observed with an additional band at 1717 cm^{-1} which is attributed to C=O stretching vibration in the carboxylic groups [46–49].

Carbon black presents similar peaks to those observed in activated carbon. A strong peak is also observed at 3432 cm^{-1} characteristic of O—H stretching vibration mode [46]. Unlike the AC case, two small bands appear at 2913 and 2850 cm^{-1} attributed to CH antisymmetric and symmetric stretching in aliphatic chains [50,51]. A medium peak at 1610 cm-1 can be ascribed to ring stretch vibration in aromatic compounds whereas a small band at 1200 cm^{-1} is assigned to lactone groups on the carbonaceous surface [46]. Conversely to AC, carbon black presents a strong peak at 1091 cm^{-1} that can be attributed to C–O stretch vibration of the C—OH bond in alcohols. Finally, a small band at 800 cm^{-1} is assigned to C—H out-of-plane bending in the aromatic rings [46, 50]. After the oxidation treatment, CBO presents additional bands at 1726 and 1380 cm^{-1}. The former belongs to C=O stretching vibration mode of carbonyl groups while the latter can be ascribed to NO_2 symmetric stretch as a consequence of the oxidation treatment with HNO_3 [50]. It is important to mention that not significant changes were observed in FTIR spectra when Ru was added on both carbon supports.

The information provided by FTIR was confirmed by Boehm's titration results (Table 1). As a result of the oxidation with HNO_3, both carbon materials increased their total acidity which means a greater amount of oxygenated groups on their surfaces. Activated carbon resulted to be a basic material since its PZC (Fig. S2) was quite high (PZC = 9.9); as a consequence; no acid sites were measured by Boehm's titration. After the functionalization through HNO_3, the amount of phenol groups and carboxylic acids increased greatly. As a result, the PZC of ACO decreased down to 4.1. The same trend was observed with carbon black. Initially, CB only possessed significantly lactones but the oxidation procedure provided additional –OH and –COOH groups to CBO surface. Since the total acidity of CBO is the highest of all assessed carbon materials, it also shows the lowest PZC because of the additional acid sites. These oxygenated functionalities on ACO and CBO surfaces can aid to the complexation of Ru during the impregnation process.

Table 2 presents the textural properties of both carbon materials. Additionally, the catalysts synthesized through wet impregnation were assessed as well to verify the impact of Ru deposition on the textural properties of both supports. AC and CB present a typical type I isotherm, indicating presence of micropores, with a bit of type IV feature as a capillary condensation occurs at high pressure with a hysteresis with the desorption, indicating the presence of large mesopores (Fig. 3) [41]. Most of AC surface area is formed by micropores created after its activation process. On the other hand, the porosity presented by CB is attributed to the interstitial spaces amid the carbon particles and nodules that form the material. AC shows a high specific surface area which is 7 times greater than that of CB. However, as regards the external surface area, the opposite is observed. The same trend is observed with pore size distribution (PSD). AC possesses pores between 0.5 and 1 nm while CB shows a wider PSD bearing pores from 2 to 75 nm. The difference of external surface area and PSD between the two assessed carbon materials is an important fact since most of AC total surface area can be wasted if oleic acid cannot diffuse inside microporosity to react with Ru in order to trigger the oxidative cleavage reaction.

Concerning the oxidation treatment, it did not affect greatly the textural properties of both carbon materials since there was only a slight decrease of their specific surface area. In addition, PSD (Fig. 3) of ACO remains almost identical to that of AC while CBO shows a narrower PSD than CB presenting since the former present pores from 2 to 27 nm. Hence, the oxidation treatment narrowed the range of pores sizes on carbon black surface. Thus, the conditions applied were ideal to incorporate oxygenated functional groups on both carbon materials without

Table 1
PZC and Boehm's titration results of carbon materials.

Support	PZC	Phenols (mmol/g)	Lactones (mmol/g)	Carboxylic acids (mmol/g)	Total Acidity (mmol/g)
AC	9.9	0.08	—	—	0.08
ACO	4.1	0.80	0.05	0.60	1.45
CB	6.9	0.06	0.54	0.04	0.64
CBO	2.9	0.43	0.52	1.02	1.97

Table 2
Textural properties of carbon materials.

Carbon Material	Specific surface area (m^2/g)	External surface (m^2/g)	Pore Volume (cm^3/g)	Mean Pore size (nm)
AC	1072	17	0.45	0.7
ACO	1017	24	0.45	0.7
ACO-Ru (2%)	994	19	0.43	0.7
CB	154	116	0.58	24.3
CBO	149	116	0.53	22.9
CBO-Ru (2%)	145	109	0.56	21.5

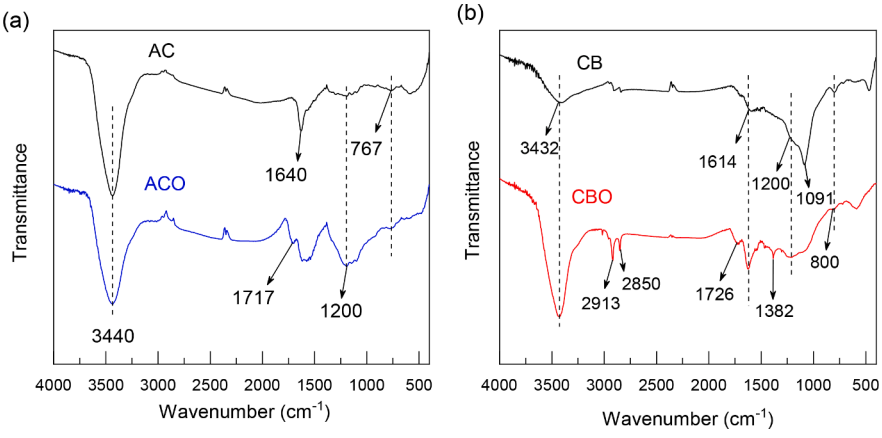

Fig. 2. (a) Infrared spectra of: (b) AC and ACO; (c) CB and CBO.

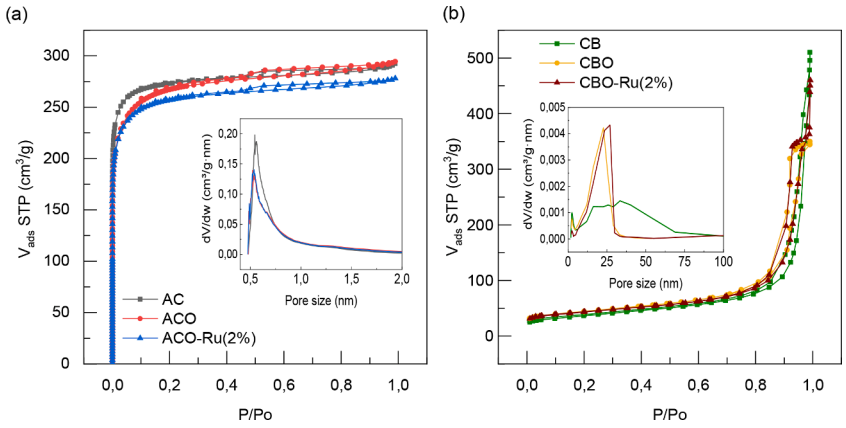

Fig. 3. N_2 adsorption-desorption isotherms of: (a) AC, ACO and ACO-Ru(2%); (b) CB, CBO and CBO-Ru(2%).

provoking great changes on their surfaces at physical level. Finally, the deposition of Ru did not produce pronounced changes on the textural properties of ACO and CBO either. As a result, two carbon catalysts with marked differences in terms of textural properties have been synthesized to evaluate their performance in the oxidative cleavage of oleic acid.

Table 3 summarizes the main characteristics of the synthesized catalysts as regards Ru deposited on ACO and CBO samples. The total load of Ru measured by ICP-AES matched with the nominal load targeted by the preparation of the catalysts. Hence, wet impregnation method was efficient for the deposition of Ru ions on both supports. On the other hand, the superficial Ru content (evaluated from XPS) was higher for both samples than their bulk content. The results provided suggest that Ru accumulates more on carbon external surface than it goes inside its porosity, which means that the carbon surface is enriched in Ru.

CO chemisorption demonstrated that CBO catalyst possesses a greater Ru dispersion than ACO-Ru(2%). Both sets of results together allow to claim that for ACO, Ru being more abundant on a smaller external surface, it tends to agglomerate more, forming bigger particles displaying a lower dispersion. Thus for the ACO based catalyst, only a third of the impregnated Ru would be available to react with oleic acid in the oxidative cleavage reaction. Nevertheless, it is important to mention that the information obtained by this technique is only indicative of the distribution of Ru on the carbon surface. Figs. S3 and S4 show XPS survey and C 1s high resolution spectra of both carbon catalysts. After deconvolution of C 1s peaks 5 contributions can be estimated: 284.8 eV (-C-H), 286.4 eV (attributed to –OH groups), 287.5 eV (C=O characteristic of carbonyl groups), 288.3 eV (ascribed to carboxylic acids) and 291.7 eV which is related to a shake-up peak. These results agree with the FTIR and Boehm's titration data (i.e. carbon supports with different oxygenated groups). Finally, Ru 3p core level (Fig. 4) displays a doublet at 464.3 and 486.4 eV which is ascribed to Ru (III) on both oxidized carbon supports [44].

Since no chlorine was detected in the survey spectrum, it is possible that the halogen was exchanged by OH groups during the impregnation process and afterwards eliminated along the several washings that the samples underwent after the impregnation.

Table 3
Ru loading on carbon catalysts.

Catalyst	Nominal Ru (wt%)[a]	Superficial Ru (wt%)[b]	Ru loading (wt%)[c]	Ru dispersion (%)[d]
ACO-Ru (2%)	2.0	8.8	1.9	33.3
CBO-Ru (2%)	2.0	4.8	1.8	47.8

[a] Nominal composition corresponding to the precursor solution.
[b] Ru superficial content determined by XPS.
[c] Ru loading determined by ICP-AES.
[d] Ru dispersion determined by CO chemisorption.

3.2. Catalytic tests

First, the oxidative cleavage of oleic acid was carried out only with $NaIO_4$ (Table 4) in order to determine to what extent the oxidizing agent could perform the reaction by itself without the solid catalyst. Then, the same procedure was performed with ACO and CBO alone (i.e. in the presence of $NaIO_4$, but without Ru in the system). Conversions resulted to be lower than 1% in all the above cases and even more no products were detected on the chromatograms. These results demonstrate that is not possible to perform the reaction with only $NaIO_4$ or the carbon supports (i.e. without Ru).

Afterwards, CBO-Ru(2%) was assessed in the oxidative cleavage reaction but with hydrogen peroxide instead of $NaIO_4$. The idea was to verify whether it was possible to perform the reaction with a softer oxidizing agent which could oxidize Ru on CBO surface. However, results were very poor. Actually, hydrogen peroxide is not strong enough to oxidize surface Ru into the species with high oxidation state required to trigger the oxidative cleavage of the carbon-carbon double bond in oleic acid.

In addition, oxidative cleavage tests were carried out with Ru(VIII)O_4 as homogeneous catalyst. In this case, $RuCl_3$ was oxidized by 8 equivalents of $NaIO_4$ into Ru(VIII)O_4. The test carried out with half of the Ru loading present on the carbon supports (i.e. 1%), achieved a complete conversion after 6 h of stirring at room temperature, while the homogeneous catalyst with the same amount of Ru as in the heterogeneous ones, completed the reaction in just 3 h of agitation.

Fig. 5 shows the performances of both carbon catalysts in the oxidative cleavage of oleic acid with 4 and 8 equivalents of $NaIO_4$. According to previous tests conducted with RuO_4 in homogeneous phase, the oxidative cleavage reaction requires at least 4 equivalents relative to the substrate to oxidize the Ru precursor salt and to fully transform oleic acid into PA and AA [9,52,53]. In spite of ACO high surface area, its catalytic activity was much lower than conversion attained with CBO-Ru (2%). When 8 equivalents of the oxidizing agent were employed, ACO-Ru(2%) showed a slight improvement in its catalytic activity. CBO-Ru(2%) performance was also greater, reaching a complete conversion after 24 h of stirring, when using 8 equivalents of $NaIO_4$.

The huge difference between the performances of the two catalysts was evidenced as well in yields and selectivity of the oxidative cleavage products. Even doubling the amount of oxidizing agent did not contribute to improve the poor yields of PA and AA when ACO-Ru(2%) was used. On the other hand, CBO-Ru(2%) shows 15% of improvement in terms of yield and selectivity after increasing the amount of $NaIO_4$ reaching values around 75%. These findings are related to the amount of nonanal and 9-oxononaoic acid present in the reaction medium. Both compounds are the precursors of PA and AA, respectively. When the

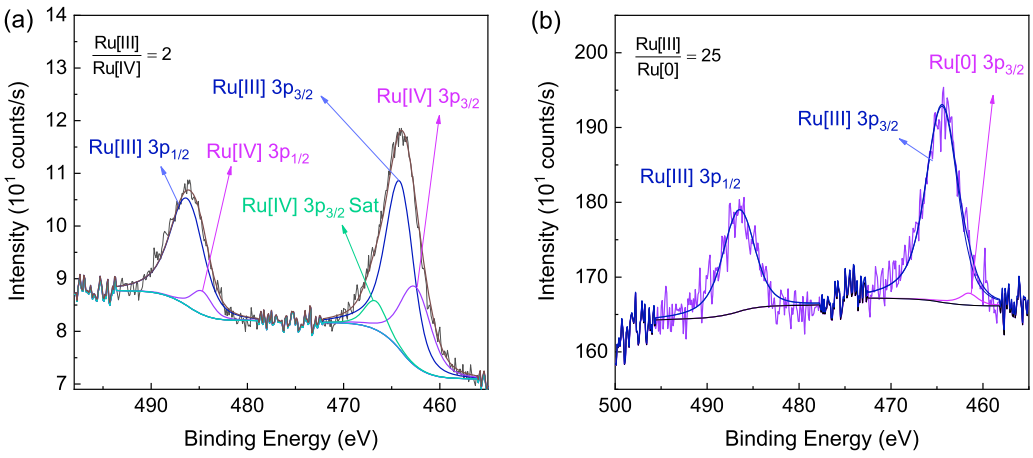

Fig. 4. Ru 3p high resolution spectra of fresh catalysts: (a) ACO-Ru(2%) and (b) CBO-Ru(2%).

Table 4
Conversion and product distribution after 24 h of stirring[a].

Catalyst	Conv. (%)	OA (%)	PA (%)	AA (%)
Blank	0.5	>99	—	—
ACO	0.4	>99	—	—
CBO	0.6	>99	—	—
CBO-PDA-Ru(2%)[b]	0.3	>99	—	—
1% RuO_4 (1.6 mg)[c]	>99	—	47.4	46.8
2% RuO_4 (3.3 mg)[d]	>99	—	48.2	48.1

[a] All tests were carried out with 141 mg of OA, 8 equivalents of $NaIO_4$, magnetic stirring for 24 h at room temperature with 100 mg of each carbon support.
[b] 3 mL of H_2O_2 instead of $NaIO_4$.
[c] Complete conversion after 6 h of stirring.
[d] Complete conversion after 3 h of stirring.

amount of $NaIO_4$ increased from 4 to 8 equivalents, the amount of both intermediates decreases in favor of the oxidative cleavage products. These findings confirm that the oxidizing agent plays an essential role in the over oxidation of the produced aldehydes after the cleavage of the oleic acid. It is worth to mention that the applied methodology (extractions, calibration curves and partition coefficient) agrees with the chemical reaction since one mole of oleic acid produces one mole of pelargonic acid and one mole of azelaic acid. Therefore, it is normal to observe identical yields and selectivities for both oxidative cleavage products.

To deepen the study of both carbon catalysts in the oxidative cleavage reaction, a hot-filtration test was conducted to verify whether the reaction was carried out by the solid catalysts. Fig. 6 confirms that in both cases an increase of catalytic activity was observed after the removal of the solid catalysts. This fact, demonstrates that Ru leached at least partially during the oxidative cleavage reaction and that leached Ru species perform the reaction. Actually, UV-Vis monitoring (Fig. 6c and d) clearly demonstrates that Ru is in form of $Ru(VIII)O_4$ (peaks at 309 and 385 nm) and as $H_2Ru(VI)O_4$ (peaks at 385 and 455 nm) species

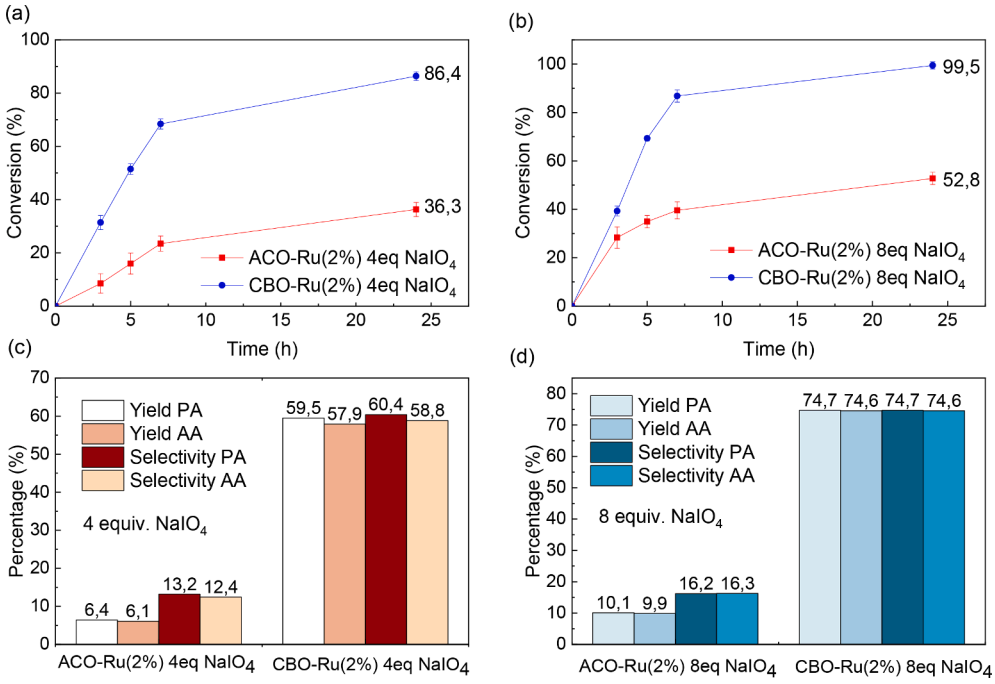

Fig. 5. Catalytic activity of ACO-Ru(2%) and CBO-Ru(2%) with (a) 4 equiv. $NaIO_4$; (b) 8 equiv. $NaIO_4$; Yields and selectivity with 0.5 mmol of OA, 100 mg of catalyst, stirring at room temperature along with (c) 4 equiv. $NaIO_4$; (d) 8 equiv. $NaIO_4$.

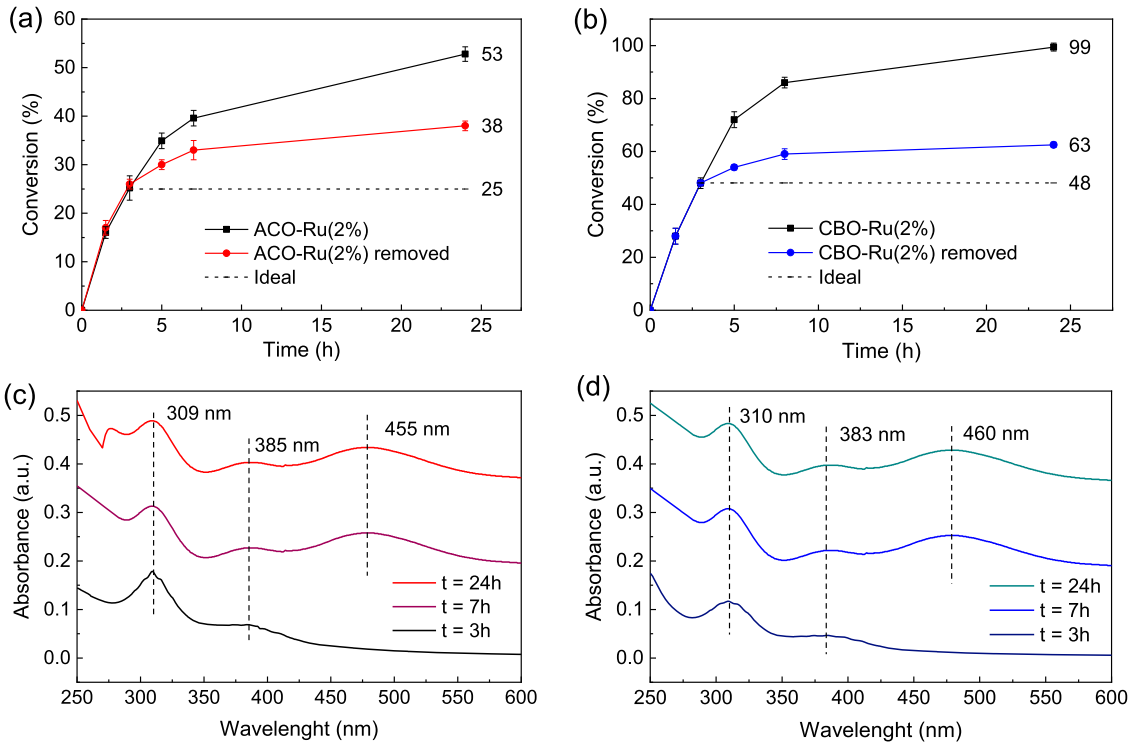

Fig. 6. Hot-filtration tests with 0.5 mmol of OA, 8 equivalents of $NaIO_4$ stirring at room temperature with 100 mg of (a) ACO-Ru(2%) and (b)CBO-Ru(2%); UV-Vis monitoring of (c) ACO-Ru(2%) and (d)CBO-Ru(2%).

[54,55]. According to literature, the former species performs the oxidative cleavage of oleic acid via a pericyclic [3+2] reaction leading to the formation of a vicinal diol (9,10 dihydroxystearic acid) and the reduced Ru species [11]. Then the diol, is cleaved by $NaIO_4$ yielding nonanal and 9-oxo nonanoic acid which are over oxidized into pelargonic and azelaic acids, respectively. $H_2Ru(VI)O_4$ can also be oxidized by means of $NaIO_4$ to maintain the catalytic activity [9,11]. Scheme 2, recapitulates the whole catalytic process.

Although an increase of catalytic activity was detected after the removal of the catalysts, the conversion accomplished at the end of the hot-filtration test was lower than when the solid catalyst was kept in the reaction medium for the whole test. Also, if Ru was acting only in the liquid phase, the results for both ACO and CBO based catalysts should have been the same regardless the chemical nature and physical properties of the supports. Hence, these results suggest that the employed support plays a role in the oxidative cleavage reaction. Among the

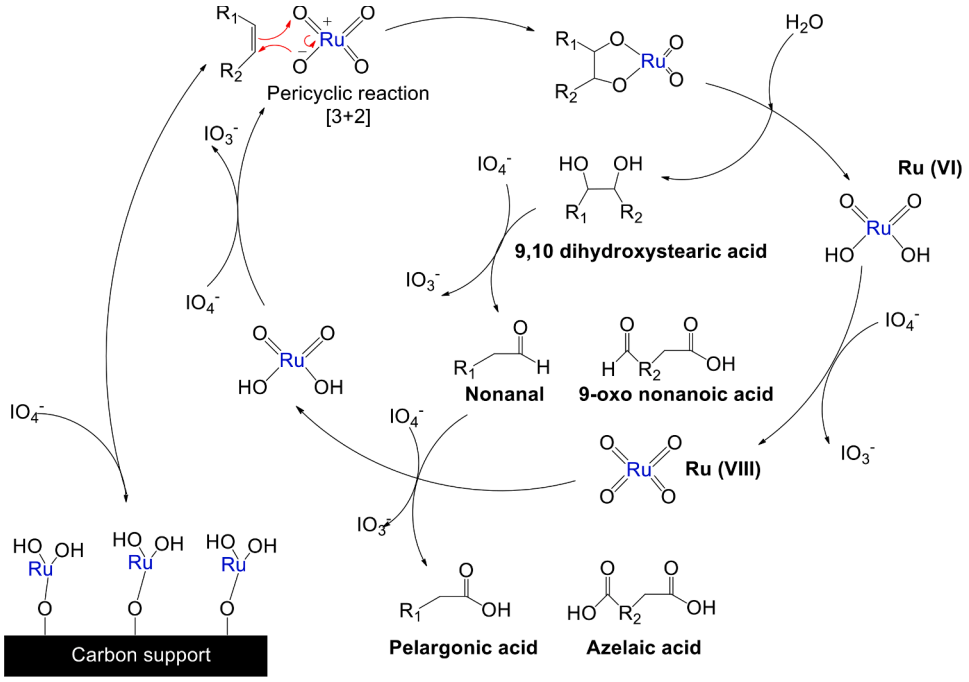

Scheme 2. Oxidative cleavage of oleic acid catalyzed by Ru-carbon catalysts.

factors explored in this work, the Ru dispersion, PSD and external surface area influence the performance of the catalysts in this reaction.

After observing the evolution with time of the yields and selectivities, it is clear that a macroporous material (and its large pore size) is preferable as compared to a support with micropores. To support this statement, the molecular size of oleic acid was estimated through an ab initio calculation using the Gaussian03 program. STO-3G minimal basis was chosen to perform the calculation with a Hartree-Fock level. The optimized molecular structure of oleic acid, depicted in Fig. 7, shows a *cis* configuration with a minimal width of 0.83 nm. It is clear then that oleic acid would hardly diffuse inside micropores of ACO (0.5 < pore size < 0.8 nm) to reach Ru located on the inner surfaces. Conversely, oleic acid molecules can diffuse easier amid the interstitial spaces of carbon black nodules improving the contact with Ru on CBO surface.

To assess the catalytic stability of both catalysts, recycling tests were conducted up to 5 times. Fig. 8 shows that ACO-Ru(2%) and CBO-Ru (2%) lose catalytic activity after each recycle. The half of the catalytic activity of ACO-Ru(2%) is lost after two recycles but thenceforth conversion is maintained around 20%. The main reason for the decrease in catalytic activity lies in Ru dissolution after its interaction with the oxidizing agent. Since the presence of Na and I was detected by XPS analysis of spent catalysts (Figs. S5 and S6), $NaIO_4$ could be one of the reasons for Ru dissolution and further oxidation into $Ru(VIII)O_4$ to trigger the oxidative cleavage reaction.

Moreover, no Ru anymore was detected by XPS after the recycling tests which demonstrates that all the available amount of the transition metal deposited on the external ACO surface got dissolved in the previous catalytic tests (Fig. 9). However, conversions achieved from third to fifth recycle runs can be due to the presence of remaining Ru on external surface and/or Ru inside micropores Most likely, Ru that was not leached in the previous catalytic tests was responsible for the activity while Ru in the micropores which is a little more protected against leaching than when it is on the external surface, can diffuse into the medium to perform the reaction. More important, ICP analysis confirmed that Ru bulk concentration of both spent catalysts is quite low which is why they show poor performances in the last recycling tests (Table 5).

The same trend was observed in the case of CBO-Ru(2%). During the first three catalytic tests, the carbon black catalyst maintained a high conversion towards the oxidative cleavage of oleic acid. This observation shows that oxygenated groups of CBO managed to maintain Ru on the surface up to three catalytic consecutive tests which is an advantage respect the homogeneous catalyst. Moreover, the supports without oxidation treatment were also submitted to recycling tests (Fig. S7). These catalysts were not active after 3 recycling tests which clearly demonstrates the benefit of carbon supports functionalization via an oxidation treatment. As regards, CBO-Ru catalyst, its catalytic activity decreases down to 38% in the last two recycling tests which confirms that Ru leached throughout the previous oxidative cleavage tests. Unlike activated carbon, XPS analyzes confirmed that Ru was still on CBO surface but yet in a much smaller quantity than before its use in the reaction (Table 5).

4. Conclusion

The oxidation treatment carried out by HNO3 did not caused excessive damages to the carbonaceous matrix of activated carbon and carbon black. Moreover, the oxidation process allowed to incorporate different oxygenated groups such as hydroxyl or carboxylic acids, on both carbon supports as it was confirmed by FTIR and Boehm's titration analyzes. The presence of oxygenated groups on activated carbon and carbon black surfaces permitted to attain the desired Ru nominal loading (i.e. 2 wt%) during the wet impregnation process, demonstrated by ICP analyzes.

The deconvolution of the XPS Ru 3p doublet allowed to estimate that the transition metal on carbon catalysts was present as Ru(III). Combined XPS and CO-chimisorption data showed that for ACO based catalyst, only a third of the impregnated Ru would be available to react with oleic acid in the oxidative cleavage reaction. This agreed with the observation that in the catalytic tests, CBO-Ru(2%) presented better catalytic activity than ACO-Ru(2%) confirming that a macroporous material is more suitable as a support than a microporous material. This claim was supported by the fact that oleic acid (*cis* configuration) has a bigger molecular size than the micropores of activated carbon which hinders the diffusion of the former inside the latter.

Hot-filtration tests demonstrated that part of Ru was present in the reaction medium after the solid catalysts were removed at approximately 50% of conversion. Through UV-Vis monitoring, it was possible to demonstrate that Ru was present as $Ru(VIII)O_4$ which is the responsible species to perform the scission of carbon-carbon double bonds by a pericyclic [3+2] reaction. The characterization of spent carbon catalysts by ICP and XPS also confirmed that Ru losses during the catalytic tests. However, CBO-Ru(2%) maintained its catalytic activity up to 3 recycling tests before to lose catalytic activity in the following catalytic tests. Moreover, macroporous CBO presented a better catalytic activity and stability than its counterpart non oxidized (i.e. CB). Thus, oxidized carbon black was identified as a promising support to perform the oxidative cleavage reaction of large UFAs which was the main purpose of this research.

Hence, the lack of homogeneity in the Ru deposition over the supports, pore sizes below the theoretical size of oleic acid and a low complexation of Ru conducted to poor performances in the oxidative cleavage of oleic acid. For all these arguments, it turned obvious the necessity to functionalize carbon black as its natural ability to retain Ru on its surface during the catalytic reaction was not strong enough.

Funding sources

"Coopération au dévelopment" doctoral program awarded to Sebastián Gámez. The project PII-DEMEX001-2018 of the Escuela Politécnica Nacional at the initial stages of the present work.

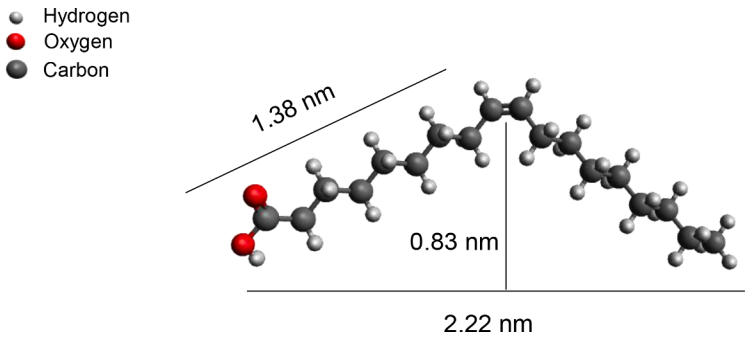

Fig. 7. Optimized geometry of oleic acid after *ab initio* Hartree-Fock calculation.

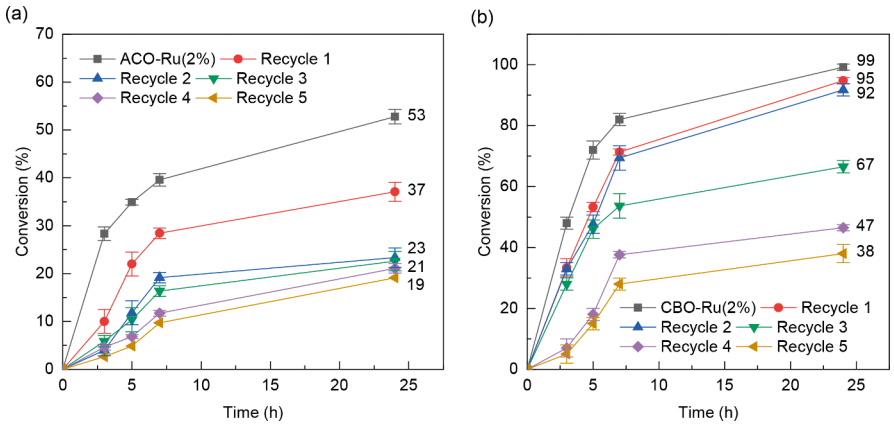

Fig. 8. Recycling tests with 0.5 mmol of OA, 8 equivalents of $NaIO_4$ stirring at room temperature with 100 mg of (a) ACO-Ru(2%) and (b)CBO-Ru(2%).

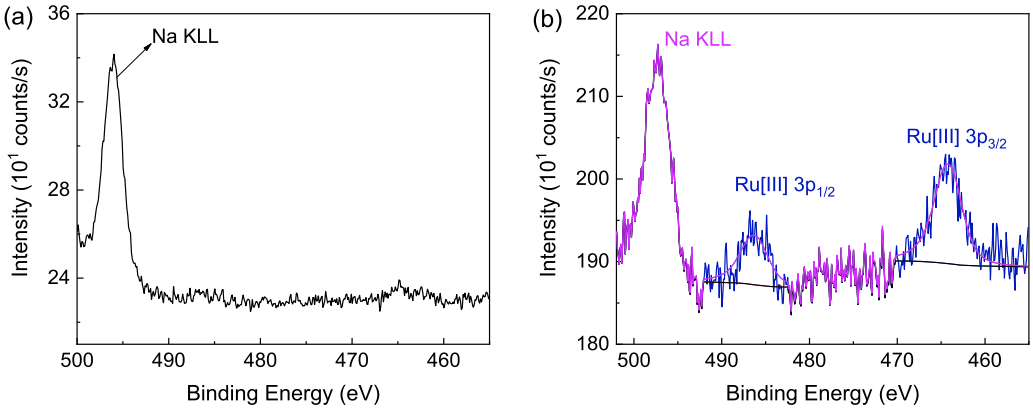

Fig. 9. Ru 3p high resolution spectra of spent catalysts: (a) ACO-Ru(2%); (b)CBO-Ru(2%).

Table 5
Ru loading on spent carbon catalysts.

Catalyst	Nominal Ru (wt%)[a]	Superficial Ru (wt%)[b]	Ru loading (wt%)[c]
ACO-Ru (2%)	2.0	—	0.5
CBO-Ru(2%)	2.0	1.7	0.8

[a] Nominal composition corresponding to the precursor solution.
[b] Ru superficial content determined by XPS.
[c] Ru loading determined by ICP-AES.

CRediT authorship contribution statement

Sebastián Gámez: Conceptualization, Methodology, Formal analysis, Writing – original draft. **Ernesto de la Torre:** Conceptualization, Writing – review & editing. **Eric M. Gaigneaux:** Project administration, Validation, Writing – review & editing.

Declaration of Competing Interest

The authors declare that they have no known competing financial interests or personal relationships that could have appeared to influence the work reported in this paper.

Data Availability

Data will be made available on request.

Acknowledgments

The authors thank the "Université catholique de Louvain" for the scholarship awarded to Sebastián Gámez in the frame of the "Coopération au développement" doctoral program. In addition, the authors address their thanks to the funding project PII-DEMEX001-2018 and of the Escuela Politécnica Nacional for the support in the initial part of the present work. We would like to acknowledge Fanny Hanon, Tommy Haynes and François Devred for achieving the scanning and transmission electron microscopies.

Supplementary materials

Supplementary material associated with this article can be found, in the online version, at doi:10.1016/j.mcat.2022.112797.

References

[1] K. Zhao, K.L. S.Liu, Z. Hu, Y. Yuan, L. Yan, H. Guo, X. Luo, Fabrication of $-SO_3H$ functionalized aromatic carbon microspheres directly from waste Camellia oleifera shells and their application on heterogeneous acid catalysis, Mol. Catal. 433 (2017) 193–201, https://doi.org/10.1016/j.mcat.2017.02.032.
[2] Y. Gao, Q. Yue, B. Gao, A. Li, Insight into activated carbon from different kinds of chemical activating agents: a review, Sci. Total Environ. 746 (2020), https://doi.org/10.1016/j.scitotenv.2020.141094.
[3] N. Zhang, L.Y. Wang, H. Liu, Q.K. Cai, Nitric acid oxidation on carbon dispersion and suspension stability, Surf. Interface Anal. 40 (2008) 1190–1194, https://doi.org/10.1002/sia.2864.
[4] O. Dutko, D. Plachá, M. Mikeska, G.S. Martynková, P. Wróbel, A. Bachmatiuk, M. H. Rümmeli, Comparison of selected oxidative methods for carbon nanotubes: structure and functionalization study, J. Nanosci. Nanotechnol. 16 (2016) 7822–7825, https://doi.org/10.1166/jnn.2016.12551.

[5] Q. Zhao, Q. Mao, Y. Zhou, J. Wei, X. Liu, J. Yang, L. Luo, J. Zhang, Chen H, Chen H, L. Tang, Metal-free carbon materials-catalyzed sulfate radical-based advanced oxidation processes: a review on heterogeneous catalysts and applications, Chemosphere 189 (2017) 224–238, https://doi.org/10.1016/j.chemosphere.2017.09.042.

[6] S. Rai, A. Ikram, S. Sahai, S. Dass, R. Shrivastav, V.R. Satsangi, Photoactivity of MWCNTs modified α-Fe_2O_3 photoelectrode towards efficient solar water splitting, Renew. Energy 83 (2015) 447–454, https://doi.org/10.1016/j.renene.2015.04.053.

[7] W.D. Wang, F. Wang, Y. Chang, Z. Dong, Biomass chitosan-derived nitrogen-doped carbon modified with iron oxide for the catalytic ammoxidation of aromatic aldehydes to aromatic nitriles, Mol. Catal. 499 (2021), https://doi.org/10.1016/j.mcat.2020.111293.

[8] A.E. Kerenkan, F. Béland, T.O. Do, Chemically catalyzed oxidative cleavage of unsaturated fatty acids and their derivatives into valuable products for industrial applications: a review and perspective, Catal. Sci. Technol. 6 (2016) 971–987, https://doi.org/10.1039/c5cy01118c.

[9] S. Rup, M. Sindt, N. Oget, Catalytic oxidative cleavage of olefins by RuO_4 organic solvent-free under ultrasonic irradiation, Tetrahedron Lett. 51 (2010) 3123–3126, https://doi.org/10.1016/j.tetlet.2010.04.040.

[10] S.E. Turnwald, M.A. Lorier, L.J. Wright, M.R. Mucalo, Oleic acid oxidation using hydrogen peroxide in conjunction with transition metal catalysis, J. Mater. Sci. Lett. 17 (1998) 1305–1307, https://doi.org/10.1023/A:1006532314593.

[11] U.S. Bäumer, H.J. Schäfer, Cleavage of olefinic double bonds by mediated anodic oxidation, Electrochim. Acta 48 (2003) 489–495, https://doi.org/10.1016/S0013-4686(02)00715-6.

[12] S. Navalon, A. Dhakshinamoorthy, M. Alvaro, H. Garcia, Heterogeneous Fenton catalysts based on activated carbon and related materials, ChemSusChem 4 (2011) 1712–1730, https://doi.org/10.1002/cssc.201100216.

[13] A. Georgi, F.D. Kopinke, Interaction of adsorption and catalytic reactions in water decontamination processes: part I. Oxidation of organic contaminants with hydrogen peroxide catalyzed by activated carbon, Appl. Catal. B Environ. 58 (2005) 9–18, https://doi.org/10.1016/j.apcatb.2004.11.014.

[14] M.S. Reza, C.S. Yun, S. Afroze, N. Radenahmad, M.S.A. Bakar, R. Saidur, A.K. Azad, Preparation of activated carbon from biomass and its' applications in water and gas purification, a review, Arab. J. Basic Appl. Sci. 27 (2020) 208–238, https://doi.org/10.1080/25765299.2020.1766799.

[15] F. Rodríguez-Reinoso, M. Molina-Sabio, M.T. González, The use of steam and CO_2 as activating agents in the preparation of activated carbons, Carbon N Y 33 (1995) 15–23, https://doi.org/10.1016/0008-6223(94)00100-E.

[16] V.Z. Radkevich, T.L. Senko, K. Wilson, L.M. Grishenko, A.N. Zaderko, V.Y. Diyuk, The influence of surface functionalization of activated carbon on palladium dispersion and catalytic activity in hydrogen oxidation, Appl. Catal. A Gener. 335 (2008) 241–251, https://doi.org/10.1016/j.apcata.2007.11.029.

[17] J. Mwila, M. Miraftab, A.R. Horrocks, Effect of carbon black on the oxidation of polyolefins-an overview, Polym. Degrad. Stab. 44 (1994) 351–356, https://doi.org/10.1016/0141-3910(94)90094-9.

[18] B.H.R. Suryanto, C. Zhao, Surface-oxidized carbon black as a catalyst for the water oxidation and alcohol oxidation reactions, Chem. Commun. 52 (2016) 6439–6442, https://doi.org/10.1039/c6cc01319h.

[19] S. Araby, Q. Meng, L. Zhang, I. Zaman, P. Majewski, J. Ma, Elastomeric composites based on carbon nanomaterials, Nanotechnology 26 (2015), https://doi.org/10.1088/0957-4484/26/11/112001.

[20] R. Alcántara, J.M. Jiménez-Mateos, P. Lavela, J.L. Tirado, Carbon black: a promising electrode material for sodium-ion batteries, Electrochem. Commun. 3 (2001) 639–642, https://doi.org/10.1016/S1388-2481(01)00244-2.

[21] L. Pahalagedara, H. Sharma, C.H. Kuo, S. Dharmarathna, A. Joshi, S.L. Suib, A. B. Mhadeshwar, Energy Fuels 26 (2012) 6757–6764, https://doi.org/10.1021/ef301331b.

[22] M.L. Studebaker, R.W. Rinehart, Infrared studies of oxygen-containing groups on the surface of carbon black, Rubber Chem. Technol. 45 (1972) 106–116, https://doi.org/10.5254/1.3544690.

[23] J.P.A. Neeft, M. Makkee, J.A. Moulijn, Catalytic oxidation of carbon black - I. Activity of catalysts and classification of oxidation profiles, Fuel 77 (1998) 111–119, https://doi.org/10.1016/S0016-2361(97)00187-7.

[24] C. Hu, X. Wang, Highly dispersed palladium nanoparticles on commercial carbon black with significantly high electro-catalytic activity for methanol and ethanol oxidation, Int. J. Hydrog. Energy 40 (2015) 12382–12391, https://doi.org/10.1016/j.ijhydene.2015.07.100.

[25] F. Wang, Y. Wang, Y. Zhang, Y. Luo, H. Zhu, Highly dispersed RuCo bimetallic nanoparticles supported on carbon black: enhanced catalytic activity for hydrogen generation from NaBH4 methanolysis, J. Mater. Sci. 53 (2018) 6831–6841, https://doi.org/10.1007/s10853-018-2013-1.

[26] M.D. Adsuar-García, J.X. Flores-Lasluisa, F.Z. Azar, M.C. Román-Martínez, Carbon-black-supported Ru catalysts for the valorization of cellulose through hydrolytic hydrogenation, Catalysts 8 (2018), https://doi.org/10.3390/catal8120572.

[27] A.V. Kumar, V.P. Reddy, R. Sridhar, B. Srinivas, K.R. Rao, An improved protocol for the oxidative cleavage of alkynes, alkenes, and diols with recyclable Ru/C, Synlett (2009) 0739–0742, https://doi.org/10.1055/s-0028-1087933.

[28] J. Cheng, L. Yu, T. Li, Y. Liu, C. Lu, T. Li, H. Wang, Effects of nanoscale carbon black modified by HNO_3 on immobilization and phytoavailability of Ni in contaminated soil, J. Chem. 2015 (2015), https://doi.org/10.1155/2015/839069.

[29] M. Toupin, D. Bélanger, Spontaneous functionalization of carbon black by reaction with 4-nitrophenyldiazonium cations, Langmuir 24 (2008) 1910–1917, https://doi.org/10.1021/la702556n.

[30] D.M. Zhou, Y.J. Wang, H.W. Wang, S.Q. Wang, J.M. Cheng, Surface-modified nanoscale carbon black used as sorbents for Cu(II) and Cd(II), J. Hazard. Mater. 174 (2010) 34–39, https://doi.org/10.1016/j.jhazmat.2009.09.012.

[31] M. Atif, R. Bongiovanni, M. Giorcelli, E. Celasco, A. Tagliaferro, Modification and characterization of carbon black with mercaptopropyltrimethoxysilane, Appl. Surf. Sci. 286 (2013) 142–148, https://doi.org/10.1016/j.apsusc.2013.09.037.

[32] American Society for Testing and Materials (ASTM), Standard Test Method for Particle Size Distribution of Granular Activated Carbon ASTM D2862, Edition June 2016. Retrieved from https://global.ihs.com/doc_detail.cfm?document_name=ASTM%20D2862&item_s_key=00017011.

[33] R. Gómez, R.L. Castro, A. Casali, S. Palma, A. Hekmat, A comminution model for secondary fragmentation assessment for block caving, Rock Mech. Rock Eng. 50 (2017) 3073–3084, https://doi.org/10.1007/s00603-017-1267-2.

[34] H.P. Boehm, Surface chemical characterization of carbons from adsorption studies. Adsorption by Carbons, Elsevier Ltd, 2008, pp. 301–327, https://doi.org/10.1016/B978-008044464-2.50017-1.

[35] S.L. Goertzen, K.D. Thériault, A.M. Oickle, A.C. Tarasuk, H.A. Andreas, Standardization of the Boehm titration. Part I. CO_2 expulsion and endpoint determination, Carbon N Y 48 (2010) 1252–1261, https://doi.org/10.1016/j.carbon.2009.11.050.

[36] N. Fiol, I. Villaescusa, Determination of sorbent point zero charge: usefulness in sorption studies, Environ. Chem. Lett. 7 (2009) 79–84, https://doi.org/10.1007/s10311-008-0139-0.

[37] T.J. Bandosz, J. Jagiello, J.A. Schwarz, Comparison of methods to assess surface acidic groups on activated carbons, Anal. Chem. 64 (1992) 891–895, https://doi.org/10.1021/ac00032a012.

[38] J.M.V. Nabais, P.J.M. Carrott, Chemical characterization of activated carbon fibers and activated carbons, J. Chem. Educ. 83 (2006) 436–438, https://doi.org/10.1021/ed083p436.

[39] J. Rouquerol, P. Llewellyn, F. Rouquerol, Is the BET equation applicable to microporous adsorbents? Stud. Surf. Sci. Catal. 160 (2007) 49–56, https://doi.org/10.1016/s0167-2991(07)80008-5.

[40] R. Brandt, R. Petricevic, H. Pröbstle, J. Fricke, Acetic acid catalyzed carbon aerogels, J. Porous Mater. 10 (2003) 171–178, https://doi.org/10.1023/A:1027486401135.

[41] F. Rouquerol, L. Luciani, Texture des Matériaux Pulvérulents ou Poreux, Techniques de l'Ingénieur, 2003, pp. 1–24. P1050(0). Retrieved from, http://cat.inist.fr/?aModele=afficheN&cpsidt=16521113.

[42] C. Nguyen, D.D. Do, The Dubinin-Radushkevich equation and the underlying microscopic adsorption description, Carbon N Y 39 (2001) 1327–1336, https://doi.org/10.1016/S0008-6223(00)00265-7.

[43] G. Horváth, K. Kawazoe, Method for the calculation of effective pore size distribution in molecular sieve carbon, J. Chem. Eng. Jpn. 16 (6) (1983) 470–475, https://doi.org/10.1252/jcej.16.470.

[44] D.J. Morgan, Resolving ruthenium: XPS studies of common ruthenium materials, Surf. Interface Anal. 47 (2015) 1072–1079, https://doi.org/10.1002/sia.5852.

[45] M.A. Vannice, The catalytic synthesis of hydrocarbons from H_2 CO mixtures over the group VIII metals. I. The specific activities and product distributions of supported metals, J. Catal. 37 (1975) 449–461, https://doi.org/10.1016/0021-9517(75)90181-5.

[46] H.F. Shurvell, Spectra- Structure Correlations in the Mid- and Far-Infrared. Handbook of Vibrational Spectroscopy, John Wiley & Sons, Ltd, 2006, https://doi.org/10.1002/0470027320.s4101.

[47] S.E. Abechi, C.E. Gimba, A. Uzairu, Y.A. Dallatu, Preparation and characterization of activated carbon from palm kernel shell by chemical activation, Res. J. Chem. Sci. 3 (2013) 54–61. https://iopscience.iop.org/article/10.1088/1757-899X/226/1/012156.

[48] A. Allwar, Characteristics of pore structures and surface chemistry of activated carbons by physisorption, FTIR and boehm methods, IOSR J. Appl. Chem. 2 (2012) 09–15, https://doi.org/10.9790/5736-0210915.

[49] S. Shin, J. Jang, S.H. Yoon, I. Mochida, A study on the effect of heat treatment on functional groups of pitch based activated carbon fiber using FTIR, Carbon N Y 35 (1997) 1739–1743, https://doi.org/10.1016/S0008-6223(97)00132-2.

[50] J.M. O'Reilly, R.A. Mosher, Functional groups in carbon black by FTIR spectroscopy, Carbon N Y 21 (1983) 47–51, https://doi.org/10.1016/0008-6223(83)90155-0.

[51] K. Kamegawa, K. Nishikubo, M. Kodama, Y. Adachi, H. Yoshida, Oxidative degradation of carbon blacks with nitric acid - II. Formation of water-soluble polynuclear aromatic compounds, Carbon N Y 40 (2002) 1447–1455, https://doi.org/10.1016/S0008-6223(01)00310-4.

[52] P.H.J. Carlsen, T. Katsuki, V.S. Martin, K.B. Sharpless, Cheminform abstract: a greatly improved procedure for ruthenium tetroxide catalyzed oxidations of organic compounds, Chem. Inf. 13 (6) (1982), https://doi.org/10.1002/chin.198206113.

[53] S. Warwel, M. Sojka, M.R.G. Klaas, Synthesis of dicarboxylic acids by transition-metal catalyzed oxidative cleavage of terminal-unsaturated fatty acids. Organic peroxygen chemistry, Top. Curr. Chem. (1993) 79–98, https://doi.org/10.1007/3-540-56252-4_26 (164). Springer, Berlin, Heidelberg.

[54] A.E.M. Boelrijk, J. Reedijk, Oxidation of methyl- and octyl-α-D-glucopyranoside, catalysed by high-valent ruthenium species; RuO_4, RuO_4^- and RuO_4^{2-}, J. Mol. Catal. 89 (1994) 63–76, https://doi.org/10.1016/0304-5102(93)E0285-O.

[55] T.J. Zerk, P.W. Moore, J.S. Harbort, S. Chow, L. Byrne, G.A. Koutsantonis, J. R. Harmer, M. Martinez, C.M. Williams, P.V. Bernhardt, Elucidating the mechanism of the Ley-Griffith (TPAP) alcohol oxidation, Chem. Sci. 8 (2017) 8435–8442, https://doi.org/10.1039/c7sc04260d.